

IMPROVED HYPERSPECTRAL IMAGING SYSTEM FOR FECAL DETECTION ON POULTRY CARCASSES

G. W. Heitschmidt, B. Park, K. C. Lawrence, W. R. Windham, D. P. Smith

ABSTRACT. *The USDA Agricultural Research Service (ARS) has developed a hyperspectral imaging system to detect fecal contaminants on poultry carcasses. The system measures the intensity of reflected light energy from about 400 nm to 1000 nm and has been used as a research tool to identify key wavelengths for detecting contaminants. Selected wavelengths are to be used in a real-time multispectral system for contaminant detection. The ARS has reported that the ratio of reflectance images at 565 nm and 517 nm was able to identify fecal contaminants. However, this ratio alone also misclassified numerous non-fecal carcass features (false positives). Recent modifications to the system, including improved lighting, a new camera, a new spectrograph, and a new algorithm with an additional wavelength, have increased fecal detection accuracy while reducing the number of false positives. The new system was used to collect hyperspectral data on 56 stationary poultry carcasses. Carcasses were contaminated with both large and small spots of feces from the duodenum, ceca, and colon, and ingesta from the crop. A total of 1030 contaminants were applied to the carcasses. The new system and algorithm correctly identified over 99% of the contaminants with only 25 false positives. About a quarter of the carcasses had at least one false positive pixel.*

Keywords. *Contaminants, Fecal, Food safety, Ingesta, Pathogen, Poultry.*

In 1996, the Food Safety and Inspection Service (FSIS) unveiled a set of requirements known as the Pathogen Reduction: Hazard Analysis and Critical Control Point (HACCP) Systems. These new food safety requirements were designed to reduce the occurrence and numbers of pathogenic microorganisms on meat and poultry products (Federal Register, 1996). Among the requirements are the establishment of controls for the prevention and removal of fecal contamination and associated bacteria. Furthermore, all meat and poultry establishments must develop and implement a system of preventative controls.

In an effort to provide these establishments with an accurate and objective means of inspecting poultry carcasses for the presence of fecal contamination, the USDA-ARS Poultry Processing and Meat Quality Research Unit initiated the development of an on-line fecal detection system. Initial research focused on the use of hyperspectral imaging to identify significant wavelengths with the goal of developing a multispectral solution suitable for poultry processing environments. A three-band common-aperture camera (MS3100, Redlake, Tucson, Ariz.) was the proposed imaging system for online integration; thus, images at up to three wavelengths could be utilized.

Hyperspectral imaging has been applied to a variety of agricultural and food inspection needs, including crop growth assessment (Yao et al., 2002), fruits ripeness (Polder et al., 2000), sugar content in melons (Tsuta et al., 2002), detection of bruises and feces on apples (Lu et al., 1999; Kim et al., 2001a; Mehl et al., 2001), wheat scab inspection (Delwiche and Kim, 2000), and food safety (Park et al., 2002a, 2002b, 2003a, 2003c; Lawrence et al., 2003; Windham et al., 2002a, 2003b, 2003c; Kim et al., 2001b). Previous research using hyperspectral imaging has shown that a ratio of reflected light at 565 nm and 517 nm resulted in high fecal detection accuracies (Park et al., 2003c; Windham et al., 2002a, 2003b, 2003c). Using these wavelengths, fecal detection accuracies ranging from 92.5% to 100% were shown to be feasible. However, Type II errors (false positives) associated with specular reflection, feathers, edge pixels, cuticle, and scabs were problematic. This article reports on efforts to reduce the number of false positives while retaining previous detection accuracies by implementing camera and lighting improvements, adding a third wavelength, and developing a new image processing method.

MATERIALS AND METHODS

MATERIALS

In each of two imaging trials, 28 birds were transported from a local poultry processing plant to the USDA-ARS Russell Research Center in Athens, Georgia, and processed on site. Prior to slaughter, birds were electrically stunned for 12 s at 50 VAC (approx. 25 mA), necks were manually cut, and birds were bled for 120 s. Carcasses were scalded at 53 °C for 120 s in a scalding tank with water recirculation and were mechanically defeathered for 30 s (D-series Picker, Stork Food Systems USA, Gainesville, Ga.). Heads and feet were removed from carcasses, and the viscera were manually removed. The gastrointestinal tract was separated into distinct

Submitted for review in December 2005 as manuscript number IET 6211; approved for publication by the Information & Electrical Technologies Division of ASABE in April 2007.

The authors are **Gerald W. Heitschmidt**, Project Coordinator, Department of Biological and Agricultural Engineering, University of Georgia, Driftmier Engineering Center, Athens, Georgia; **Bosoon Park**, **ASABE Member Engineer**, Agricultural Engineer, **Kurt C. Lawrence**, **ASABE Member Engineer**, Agricultural Engineer, **William R. Windham**, Animal Physiologist Scientist, and **Doug P. Smith**, Research Food Technologist, USDA-ARS Russell Research Center, Athens, Georgia **Corresponding author:** Bosoon Park, USDA-ARS Russell Research Center, P.O. Box 5677 Athens, GA 30604-5677; phone: 706-546-3396; fax: 706-546-3633; e-mail: bosoon.park@ars.usda.gov.

areas using clamps, and contents removed from the crop and gizzard (ingesta), duodenum, ceca, and colon. Contents were kept in plastic vials until applied to the carcasses.

Camera System

The camera system employed in the previous studies was a visible/near-infrared hyperspectral imaging system (ITD, Stennis Space Center, Miss.). This system had several key components, including a 12-bit SensiCam SVGA camera (Cooke Corporation, Auburn Hills, Mich.) with a 1/2 in. format, 1280 × 1024 pixel, thermoelectrically cooled (Peltier) CCD. The spectrograph was an ImSpector V9 (Specim, Oulu, Finland) with a 25 micron entrance slit and wavelength range of 430 to 900 nm. In addition, the front lens was a 1.4/17 mm compact format C-mount Xenoplan (Schneider Optics, Hauppauge, N.Y.). Image scanning was performed using a focal plane scanner that moved the front lens in a vertical motion relative to the spectrograph's entrance slit. During the scanning process, lines of spatial data were collected wherein each pixel in the captured line containing a complete reference spectrum. Due to inherent optical characteristics of this spectrograph, smile and keystone distortions were observed in the resulting hyperspectral data cubes, and methods were developed to try to rectify these distortions (Lawrence et al., 2001). Although these efforts reduced smile and keystone effects in the imagery, distortions often persisted in isolated areas of the imagery. These distortions manifested themselves in the form of band-to-band misregistration that increased in severity with increased distance between wavelength centers. These misregistration errors could significantly impact the ability to detect small fecal spots using band ratios. To address this problem, a new hyperspectral imaging system was developed and is described below.

The new hyperspectral imaging system employed in this study utilized a 12-bit SensiCam QE camera (Cooke Corporation, Auburn Hills, Mich.). This camera was outfitted with a 2/3 in. format, 1376 × 1040 pixel, Peltier-cooled CCD array; thus, it offered a slight increase in both spectral and spatial resolution over the previous system. More importantly, the QE offered improved quantum efficiency across the spectrum relative to the SVGA model. The spectrograph was upgraded to an ImSpector V10E (Specim, Oulu, Finland) with a 30 micron entrance slit and wavelength range of 400 to 1000 nm. This new spectrograph reduced smile and keystone errors to a point (<5 μm) where geometric corrections were no longer required. Resulting spatial distortions were

less than 0.5 pixels at the image edges when comparing short and long wavelengths. Finally, the front lens was upgraded from a small to large format C-mount lens (XNP 14/23-0302, Schneider Optics, Hauppauge, N.Y.), which enabled improved image acuity through easier focusing.

In addition to the hyperspectral imaging system, a digital video camcorder (DCR-TRV900, Sony Corp., Tokyo, Japan) recorded the application, location, areal extent, and type of each contaminant as they were applied to the poultry carcasses in order to aid in the accuracy assessment. Other features of interest, such as feathers, scabs, scratches, etc., were also documented on the video.

Lighting

Park et al. (2003b) used a pair of 150 W tungsten-halogen fiber-optic illuminators and line lights (A-240, Dolan-Jenner, Inc., Lawrence, Mass.) positioned lateral to the carcass's keel. While providing sufficient illumination intensity at 517 nm and 565 nm, the angles of illumination resulted in observed shadowing in the wing and vent cavities. Although ratio-based algorithms are advantageous for processing imagery containing shadows, intense shadowing can result in low signal-to-noise values and decrease the algorithm's efficacy.

Because the vent area of the poultry carcass is particularly prone to contamination, in the current study a series of six DC-stabilized light sources (MR1600, Gilway Technical Lamp, Woburn, Mass.) were positioned surrounding the hyperspectral imaging system, targeting the vent and wing cavity areas (fig. 1). Each light source was outfitted with a 35 W MR16 tungsten-halogen lamp (22° beam spread) and a frosted glass diffusion filter. The direct illumination prevented wingtips and other protruding features from casting shadows in the vent and wing cavities. Each light was positioned with a working distance equal to that of the camera (78.7 cm), thus ensuring that the light fixtures and camera could all eventually reside in a protective NEMA 4x stainless steel cabinet suitable for poultry processing plants.

METHODS

Hyperspectral images were collected by hanging each carcass on a dedicated static shackle at a 78.7 cm (31 in.) nominal working distance. The four types of contaminants were then applied to each carcass. Each contaminant was applied in multiple locations on the carcasses using both large and small spots (fig. 2). Particular attention was given to the vent,

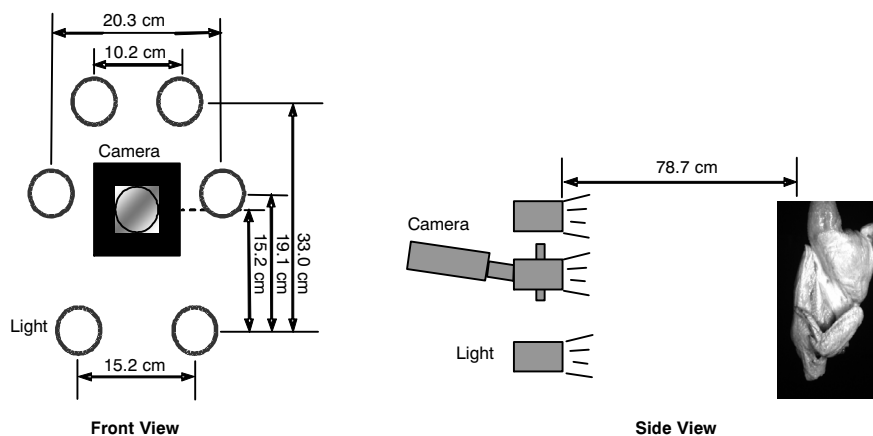


Figure 1. Diagram of hyperspectral camera and lighting.

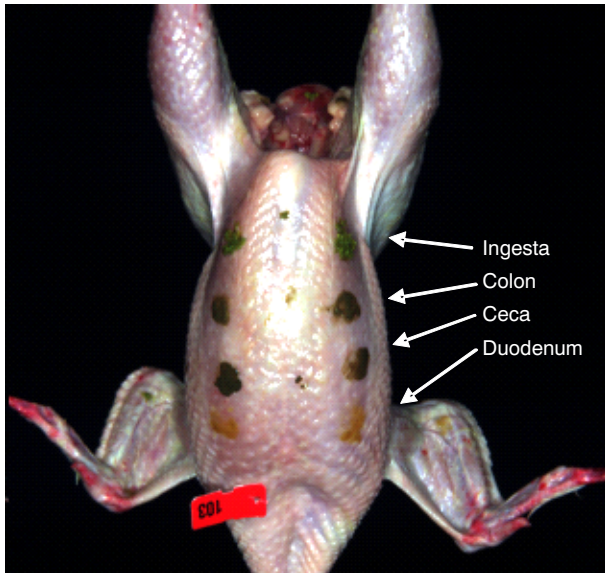


Figure 2. Carcass shown with contaminants applied.

wing cavity, and breast areas. A total of 477 contaminant spots were applied to the first set of 28 birds, and 553 spots to the second set.

In order to obtain a suitable view of the carcass vent area, the hyperspectral imaging system was positioned slightly above the vent and angled towards the center of the keel. This positioning provided a shallow look angle that brought the vent area into the imaging system's field of view while preserving the view of the remaining frontal area of the carcass.

HyperVisual software (ITD, Stennis Space Center, Miss.) was used to image carcasses, both clean and contaminated. Camera binning was set at 4×2 (vertical pixels \times horizontal pixels), resulting in images with 344 columns and 520 spectral bands. Using the system's focal plane scanner, 300 lines were scanned, with an integration time of 30 ms per line. Each image was then calibrated to percent reflectance using a dark current image and an image of a 30.5×30.5 cm (12×12 in.) 99% Spectralon calibration standard (SRT-99-120, Labsphere, North Sutton, N.H.). Carcass images were calibrated to percent reflectance with:

$$R = \left[\frac{\text{observed} - \text{dark}}{\text{reference} - \text{dark}} \right] * 100 \quad (1)$$

where

observed = carcass image
dark = dark current image
reference = Spectralon image.

This calibration was applied at each pixel location and at each wavelength with HyperVisual software. Next, images were spectrally smoothed with a nine-point moving average. The final preprocessing step was to create two large mosaics containing 28 carcass images each. This approach produced a single image for each trial where image processing routines could be quickly applied to all 28 birds and offered a quick, synoptic view of the results. The mosaicking and subsequent image processing steps were performed with ENVI software (Research Systems, Inc., Boulder, Colo.).

RESULTS AND DISCUSSION

IMAGE PROCESSING

Because online inspection would be performed using a three-band common-aperture camera (MS3100, Redlake, Tucson, Ariz.), it was possible to utilize a third wavelength to improve contaminant detection relative to previous studies. To select a third wavelength, a statistical analysis was performed on the mean spectra from the contaminants and various clean features on the carcasses. For each carcass image, regions of interest (ROI) were selected, as described by Windham et al. (2002b), at seven different locations: uncontaminated skin from the thigh, breast, and wing portions of the carcasses, and duodenum, ceca, colon, and ingesta contaminants applied to the carcass ($N = 196$). ROIs are simply a group of pixels, often contiguous, that collectively define a feature of interest to the researcher. Additionally, ROIs of cuticle ($N = 6$) were selected from six carcasses from which the cuticle was not totally removed by immersion scalding. Cuticle, an outer layer of skin (stratum corneum) containing yellow pigments, was often the source of false positives using the two-band ratio. The mean ROI reflectance spectra at each wavelength were calculated.

A single-term linear regression (STLR) program (Windham et al., 2003a) was used to analyze the ROI spectra ($N = 202$). The STLR program uses equation 2 to search the spectral data to find the optimum set of reflectance values (R_{λ_i}) at a given wavelength (λ_i) that are highly correlated with the dependent variable:

$$B = f \left[\frac{(R_{\lambda_1} - R_{\lambda_2})}{(R_{\lambda_3} - R_{\lambda_2})} \right] \quad (2)$$

where B is the arbitrary constituent value (1 for uncontaminated skin, and 2 for feces/ingesta), and R_{λ} is the reflectance at wavelength λ_i .

Because λ_1 and λ_3 were known (565 nm and 517 nm, respectively), only λ_2 needed to be determined by the STLR program. The in-house STLR program computed the correlation coefficient (r) at every available wavelength, given λ_1 and λ_3 . The corresponding r was then plotted against wavelength, giving a "correlation plot" of r vs. wavelengths (Williams and Norris, 2001). The wavelength giving the best r was thus "optimized" for λ_2 , given λ_1 and λ_3 . When this technique was applied to the calibration sample set, a maximum correlation of 0.87 was found for the quotient of differences with λ_2 at 802 nm. Although fecal and ingesta detection was determined to be comparable to the 565/517 nm ratio, incorporating the pixel-based $R_{\lambda_{802}}$ data into equation 2 resulted in a significant number of false positives. This was especially true for feathers and edge pixels. In order to utilize $R_{\lambda_{802}}$, a new method was required to preserve the 565/517 nm ratio and reduce false positives. Thus, development of a decision tree classifier was undertaken (fig. 3).

The decision tree classifier used a series of binary decisions to separate pixels into classes. Each decision, or node, divided the pixels in an image into two classes based on a user-defined expression. In this case, each node contained a conditional statement designed to determine a given pixel's likelihood of being a contaminant or some other type of feature often spectrally confused with contaminants. In this way, pixels that were problematic for the 565/517 nm ratio could

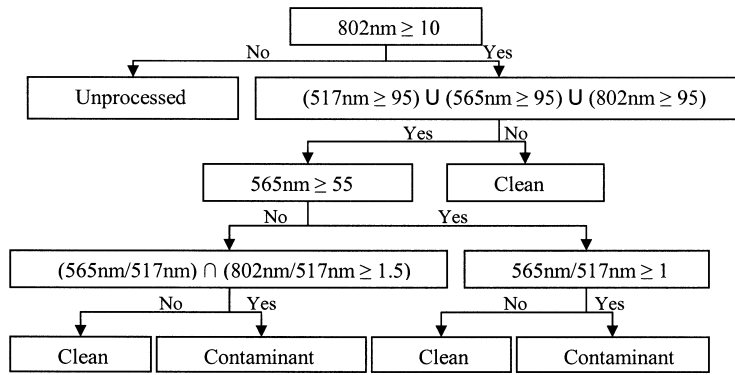


Figure 3. Diagram of the decision tree classification procedure.

be identified and “redirected” for separate consideration. In addition, the third wavelength could be introduced to further reduce false positives while preserving the predictive power of the 565/517 nm ratio.

As shown in figure 3, the first step in the process was to mask the feature space to be examined. This was accomplished simply by setting a threshold for the image collected at 802 nm that would include poultry features while excluding the background feature space. The resulting binary mask was then eroded using a 5×5 kernel to eliminate pixels along the edge of the carcass from examination, as they were occa-

sionally the source of false positives in previous studies. More importantly, this step removed protruding feathers from the image’s feature space (fig. 4). Feathers that remained on the carcass after processing were most often located along the wing perimeter and would spectrally mix with the background, resulting in false positives, and were thus eliminated from analysis with this approach. However, the feathers must be along the carcass perimeter in order for this processing to be effective.

After masking, the remaining pixels were checked for specular reflection. Specular pixels, typically with reflec-

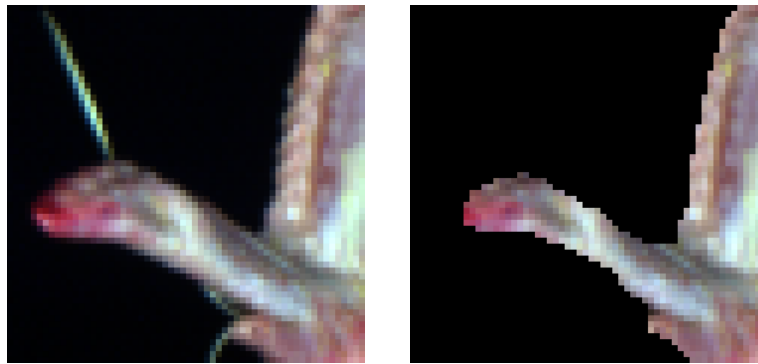


Figure 4. Edge pixels and feathers on wing (left) are removed after masking (right).

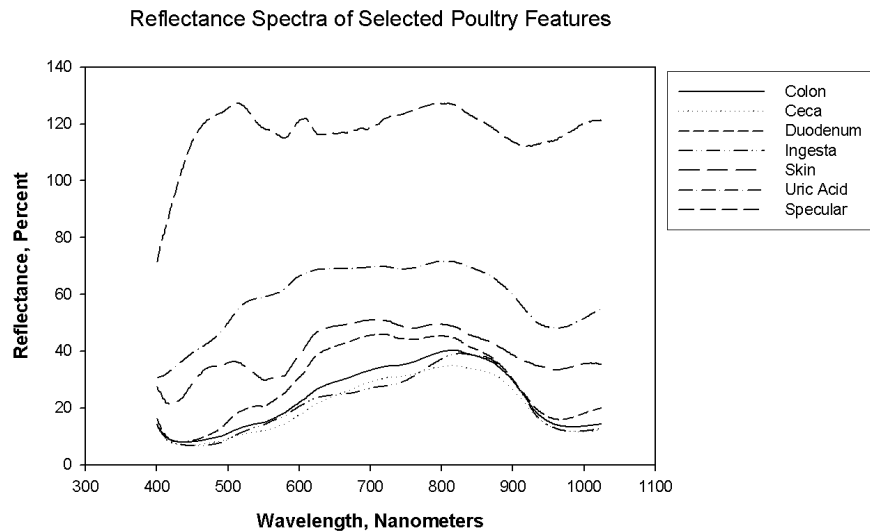


Figure 5. Average reflectance spectra of selected carcass features.

tance values approaching or exceeding 100%, yielded highly inconsistent and varied spectral responses. These pixels were the product of wet, uncontaminated surface features on the carcasses. Therefore, pixels with reflectance values $\geq 95\%$ were classified as clean. Figure 5 shows the average reflectance values of all pixels that were $\geq 95\%$ in at least one of the three designated wavelengths, as well as the mean reflectance of the most highly reflective contaminant: colon samples possessing a high concentration of uric acid. The reflectance values associated with specular reflection were significantly higher than that of colon with a high concentration of uric acid and could thus be differentiated.

Those pixels not classified as clean were then tested for the presence of concentrated uric acid. In a very small number of colon samples, significant concentrations of uric acid were present. Uric acid appears as a white pasty substance, much brighter in reflectance than the typical contaminant. Figure 5 shows the reflectance values of uric acid to be higher than those of the typical contaminant, but lower than that of specular reflection. Because uric acid spectra had a positive slope between 517 nm and 565 nm, the 565/517 nm ratio was capable of detecting this contaminant. However, when integrating an 802 nm image to eliminate various false positives, the uric acid was not detected. Thus, a threshold ($\geq 55\%$ at 565 nm) was established whereby pixels with reflectance values indicative of uric acid could be processed by the 565/517 nm ratio alone (uric acid test in fig. 3).

The remaining pixels, those that possessed reflectance values less than 55% at 565 nm, were processed with the following conditional statement:

$$\left(\frac{R_{\lambda_{565}}}{R_{\lambda_{517}}} \geq 1.05 \right) \cap \left(\frac{R_{\lambda_{802}}}{R_{\lambda_{517}}} \geq 1.5 \right) \quad (3)$$

Using this conditional statement, a given pixel must be identified as a contaminant in both cases in order to be classified as a contaminant. Although the 802/517 nm ratio accurately detected fecal contamination, it also produced abundant false positives. However, it was not sensitive to cuticle. Therefore, when using these ratios in combination, fecal contaminants were retained while cuticle was eliminated, which was a significant problem in earlier research (Park et al., 2003c). The 1.05 threshold for the 565/517 nm was based on previous research, while the 1.5 threshold for the 802/517 nm ratio was determined by trial and error. Figure 6 shows the results of the 565/517 nm ratio on a carcass with a pronounced cuticle remnant incorrectly identified as a contaminant on the keel. Figure 7 shows the results of the decision tree, with the cuticle eliminated and the true contaminants correctly classified.

Using high-resolution digital video and still pictures as a guide, a ground truth image was generated and used as a baseline against which the results of the decision tree could be validated. Table 1 shows the accuracies of both 28-bird trials, plus their combined totals. Detection of contaminants averaged just better than 99% for both studies combined. These accuracies are consistent with earlier research (Park et al., 2003b, 2003c). The number of contaminants omitted totaled just 10 out of 1030. In contrast to earlier studies, the percentage of birds containing at least a single-pixel false positive was 28.57%, representing a significant improvement. More specifically, there were 25 false positives distributed among 16 birds. Most of the false positives were single-pixel errors.

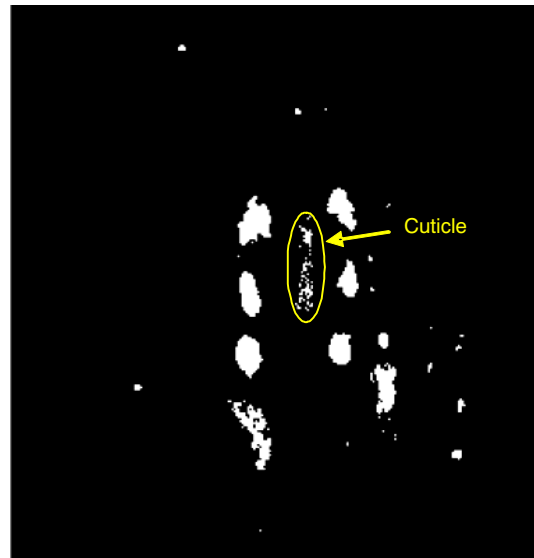


Figure 6. Results of 565/517 nm ratio image alone.

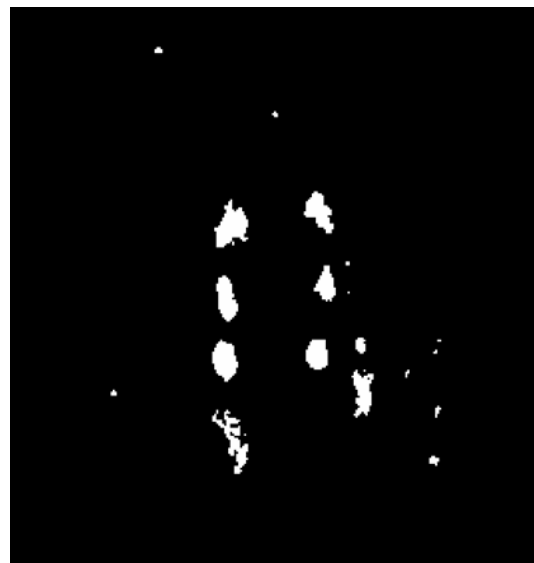


Figure 7. Results of decision tree classifier.

False negatives were largely associated with duodenum. Because feces extracted from the duodenum were typically runny in consistency, they tended to flow down the carcass prior to imaging. This dispersion process resulted in a blending of the contaminant with the carcass skin, making detection difficult where concentrations were thin. Indeed, nine out of the ten false negative errors were associated with duodenum “runs.”

False positive errors were generally associated with feathers and small scabs. Although many of the feathers were

Table 1 Tabulation of the accuracies from both 28-bird studies.

	Study 1	Study 2	Totals
Correct (%)	99.4	98.7	$\mu = 99$
False negatives (%)	0.6	1.3	$\mu = 0.9$
Correct (No.)	474 (of 477)	546 (of 553)	1020 (1030)
False negatives (No.)	3	7	10
False positives (No.)	18	7	25
Birds w/false pos. (No.)	11	5	16
Birds w/false pos. (%)	39.3	17.9	28.6

eliminated from testing through the masking process, a few feathers remained in the feature space because they were positioned anterior to the carcass rather than laterally as shown in figure 4. Thus, these feathers survived the masking process. Although most scabs did not cause false positives, a few small scabs did.

CONCLUSIONS

A combination of hardware and software changes has improved the overall performance of contaminant detection based on data collected with a hyperspectral imaging system. Using a spectral subset of just three wavelengths, a high rate of detection (>99%) is possible, while reducing the frequency and extent of false positives relative to previous research. Most false positives were of the single-pixel-per-bird variety. While these small false positives can be easily filtered out, it may not be desirable to do so, since an aggregate of several single-pixel true positives could indicate a contaminant problem. The feathers and scabs that resulted in false positives presented no discernable spectral pattern; thus, preventing them will present a challenge.

The current state of the art prevents the use of hyperspectral solutions for on-line inspection. As such, hyperspectral imaging may continue to serve as a valuable research tool in the laboratory, while multispectral derivatives should continue to seek ways to further reduce false positives.

ACKNOWLEDGEMENTS

The authors would like to thank Peggy Feldner, Food Technologist; Alan Savage, Engineering Technician; Preston Snead, Information Technology Specialist; and Steven Upchurch, Computer Specialist, for their assistance in poultry processing and data collection.

REFERENCES

- Delwiche, S. R., and M. S. Kim. 2000. Hyperspectral imaging for detection of scab in wheat. *Proc. SPIE* 4203: 13-20.
- Federal Register. 1996. Pathogen reduction: Hazard Analysis and Critical Control Point (HACCP) systems; Final Rule. *Federal Register* 61(144).
- Kim, M. S., K. Chao, Y.-R. Chen, D. Chan, and P. Mehl. 2001a. Hyperspectral imaging system for food safety: Detection of fecal contamination on apples. *Proc. SPIE* 4206: 174-184.
- Kim, M. S., Y. R. Chen, and P. M. Mehl. 2001b. Hyperspectral reflectance and fluorescence imaging system for food quality and safety. *Trans. ASAE* 44(3): 721-729.
- Lawrence, K. C., B. Park, W. R. Windham, and C. Mao. 2001. Calibration of imaging spectrometry system for inspection of contaminated poultry carcasses. ASAE Paper No. 013129. St. Joseph, Mich.: ASAE.
- Lawrence, K. C., B. Park, W. R. Windham, and C. Mao. 2003. Calibration of a pushbroom hyperspectral imaging system for agricultural inspection. *Trans. ASAE* 46(2): 513-521.
- Lu, R., Y. R. Chen, B. Park, and K. H. Choi. 1999. Hyperspectral imaging for detecting bruises in apples. ASAE Paper No. 993120. St. Joseph, Mich.: ASAE.
- Mehl, P. M., K. Chao, M. Kim, and Y.-R. Chen. 2001. Detection of contamination on selected apple cultivars using reflectance hyperspectral and multispectral analysis. *Proc. SPIE* 4206: 201-213.
- Park, B., K. C. Lawrence, W. R. Windham, and D. P. Smith. 2002a. Multispectral imaging system for fecal and ingesta detection on poultry carcasses. ASAE Paper No. 023138. St. Joseph, Mich.: ASAE.
- Park, B., W. R. Windham, K. C. Lawrence, D. P. Smith, and P. W. Feldner. 2002b. Hyperspectral imaging for food processing automation. *Proc. SPIE* 4816: 308-316.
- Park, B., K. C. Lawrence, W. R. Windham, and D. P. Smith. 2003a. Assessment of hyperspectral imaging system for poultry safety inspection. *Proc. SPIE* 4879: 269-279.
- Park, B., K. C. Lawrence, W. R. Windham, D. P. Smith, and P. W. Feldner. 2003b. Machine vision for detecting internal fecal contaminants of broiler carcasses. ASAE Paper No. 033051. St. Joseph, Mich.: ASAE.
- Park, B., K. C. Lawrence, W. R. Windham, and R. J. Buhr. 2003c. Hyperspectral imaging for detecting fecal and ingesta contaminants on poultry carcasses. *Trans. ASAE* 45(6): 2017-2026.
- Polder, G., G. W. A. M. van der Heijden, and I. T. Young. 2000. Hyperspectral image analysis for measuring ripeness of tomatoes. ASAE Paper No. 003089. St. Joseph, Mich.: ASAE.
- Tsuta, M., J. Sugiyama, and Y. Sagara. 2002. Near-infrared imaging spectroscopy based on sugar absorption for melons. *J. Agric. Food Chem.* 50(1): 48-52.
- Williams, P., and K. Norris. 2001. *Near-Infrared Technology in the Agricultural and Food Industries*, 46. 2nd ed. St. Paul, Minn.: American Association of Cereal Chemists.
- Windham, W. R., D. P. Smith, B. Park, and K. C. Lawrence. 2002a. Algorithm development from visible/NIR spectra for detection of poultry feces and ingesta. ASAE Paper No. 026032. St. Joseph, Mich.: ASAE.
- Windham, W. R., K. C. Lawrence, B. Park, D. P. Smith, and G. Poole. 2002b. Analysis of reflectance spectra from hyperspectral images of poultry carcasses for fecal and ingesta detection. SPIE Paper No. 4816-36.
- Windham, W. R., D. P. Smith, B. Park, and K. C. Lawrence. 2003a. Algorithm development with visible/near infrared spectra for detection of poultry feces and ingesta. *Trans. ASAE* 46(6): 1733-1738.
- Windham, W. R., K. C. Lawrence, B. Park, L. A. Martinez, M. A. Lanoue, D. A. Smith, J. Heitschmidt, and G. H. Poole. 2003b. Method and system for contaminant detection during food processing. U.S. Patent No. 6587575.
- Windham, W. R., K. C. Lawrence, B. Park, and R. J. Buhr. 2003c. Visible/NIR spectroscopy for characterizing fecal contamination of chicken carcasses. *Trans. ASAE* 46(3): 747-751.
- Yao, H., L. Tian, M. Paulsen, A. Kaleita, and M. Singh. 2002. Hyper-spectral imagery for various crop growth information extract ion. ASAE Paper No. 021076. St. Joseph, Mich.: ASAE.